Keck Adaptive Optics Note (KAON) 496

Atmospheric turbulence statistics from the MASS/DIMM unit (T6) at the Mauna Kea 13 North site: Update no. 2 (06/29/07)

Ralf Flicker *(rflicker@keck.hawaii.edu)*
Christopher Neyman *(cneyman@keck.hawaii.edu)*
W. M. Keck Observatory, 65-1120 Mamalahoa Hwy., Kamuela, HI 96743

29 June 2007

Non-disclosure statement

This analysis was performed by kind permission of the TMT who provided access to the T6 data archives for the Keck Adaptive Optics group and NGAO collaboration. As of the time of publication of this document and until TMT has made the data public, the information disclosed in this document must under no circumstances be distributed or communicated to the public.

Acknowledgements

We are grateful to the following people for granting us access to their atmospheric data measurement sets and helping us with parts of the analysis: Matthias Schöck, Warren Skidmore and Sebastian Egner at TMT; Ryan Lyman and Tiziana Cherubini at MKWC; Fumihiro Uraguchi (Subaru), Mark Chun (UH) and Jim Thomas (CFHT).

1 Introduction

This document is an update of KAON 415 which presented a first cut of the data analysis, spanning the June 2005 to August 2006 time frame. For the current update, the data set was extended to include the most recent entries in June 2007. The document now also includes a previously unpublished addendum (Sect. 2) that compares the T6 statistics to contemporaneous seeing and turbulence measurements gathered by other observatories on the Mauna Kea summit. Since this is an update of a previously published study, the reader is referred to the original document (KAON 415 on Keckshare) for background material and other details concerning the data format and the analysis. Only the latest statistics obtained from applying the previously developed IDL analysis script to the extended data set are presented here.

Parameter		mean	25%	median	75%	unit
Seeing	θ	0.880	0.576	0.749	1.028	arc seconds
Fried parameter	r_0	0.141	0.098	0.135	0.175	meters
Isoplanatic angle	θ_0	2.799	1.902	2.621	3.473	arc seconds
Focal anisoplnatism	d_0	5.080	3.390	4.720	6.331	meters
Free atmosphere r_0	r^*	0.359	0.174	0.299	0.474	meters
Greenwood frequency	f_G	54.30	17.89	38.18	93.71	Hz

Table 1: statistical parameters of 13 N: Mean, 25, 50 and 75 percentiles (of the cumulative density function, CDF) of the principal turbulence parameters extracted from the MASS/DIMM data. Refer to Sect. A for definitions of the parameters.

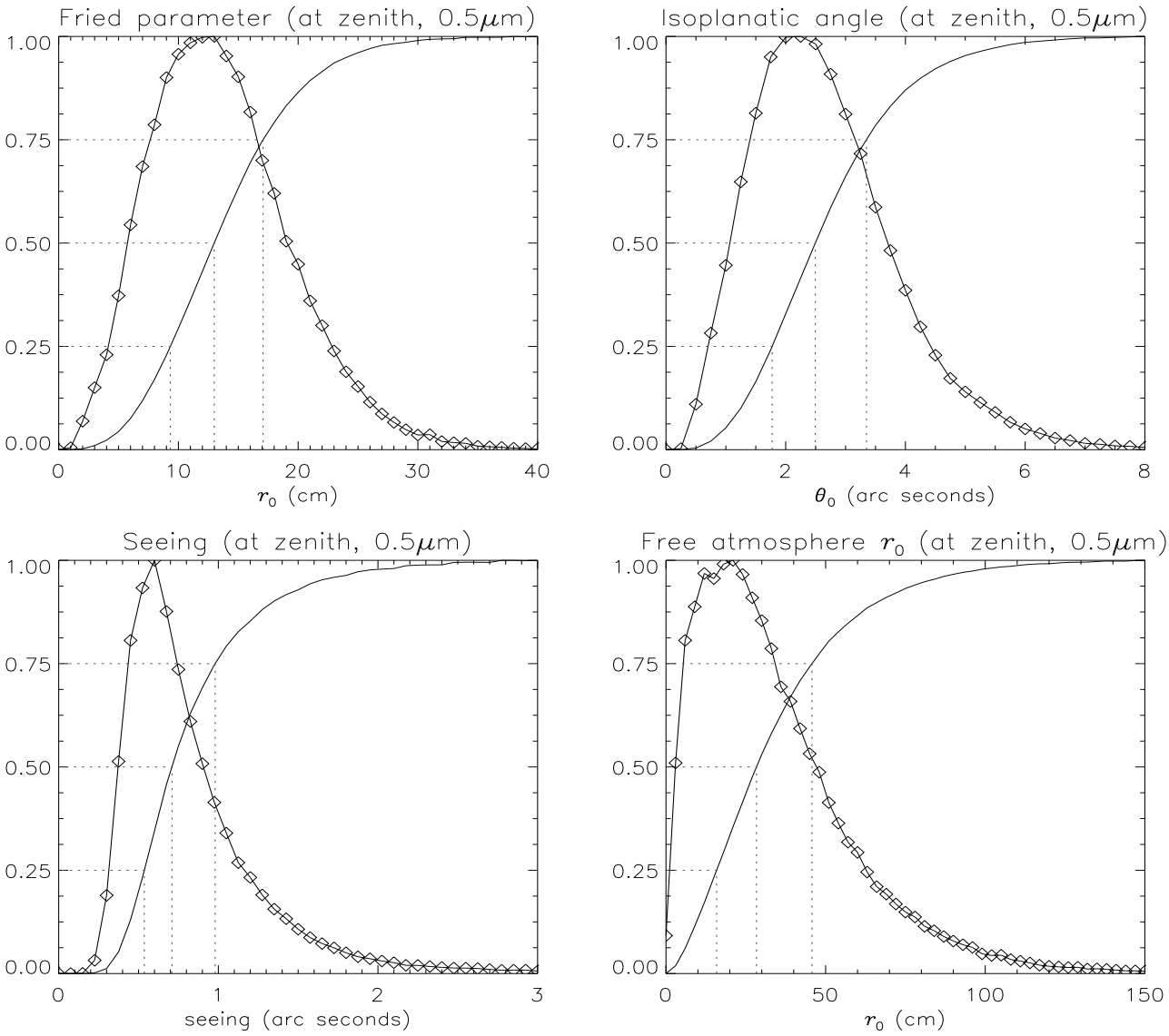

Figure 1: Histograms (solid line plus diamond plot symbols) and cumulative density functions (CDFs) of the main atmospheric parameters. The y-axes are scaled to the CDFs, and the density functions have been scaled up (from unit integral) for display purposes. The three lines in each graph mark the 25th, 50th and 75th percentiles.

Altitude (m)	0	500	1000	2000	4000	8000	16000
MEAN							
c_l ($m^{1/3}$)	3.95e-13	4.93e-14	2.59e-14	2.52e-14	4.35e-14	3.37e-14	2.22e-14
c_l/μ_0	0.664	0.083	0.043	0.042	0.073	0.0 57	0.037
50% MEAN							
c_l ($m^{1/3}$)	3.46e-13	4.23e-14	1.73e-14	2.23e-14	3.71e-14	2.64e-14	1.96e-14
c_l/μ_0	0.677	0.082	0.034	0.044	0.073	0.052	0.038

Table 2: Mean turbulence profiles at zenith, as represented by the integrated layer coefficients $c_l$and the fractional layer contribution c_l/μ_0. Refer to Sect. A for definitions of the parameters. The second group called "50% mean" is the profile based on a box around the peak of the joint $\{r_0, \theta_0\}$ histogram (see Figs. 2 and 3), between the 25 and 75 percentile r_0 and θ_0 values.

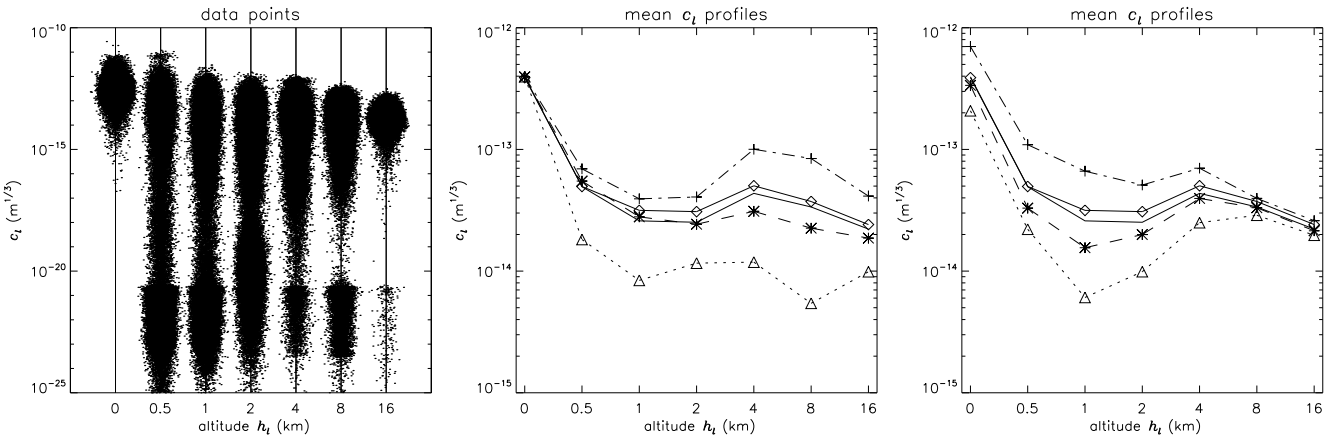

Figure 2: Left: density plot (or "cloud plot") of the c_l coefficients as returned by the MASS. For visualization purposes, the data points corresponding to each altitude have been smeared out around the central x-value by a Gaussian distribution, in order to make the impression of density clearer to the eye. Middle and right: average turbulence profiles, in various sub-sets of r_0 and θ_0 statistics. The solid line without symbols is the average of each c_l over the entire data set. The asterisks are averages over the central 50% set, pluses and triangles are averages over the 25% sets on either side of the 25th and 75th percentiles, and diamonds are averages over a 50% set from the two- dimensional joint $\{r_0, \theta_0\}$ histogram (see Fig. 3).

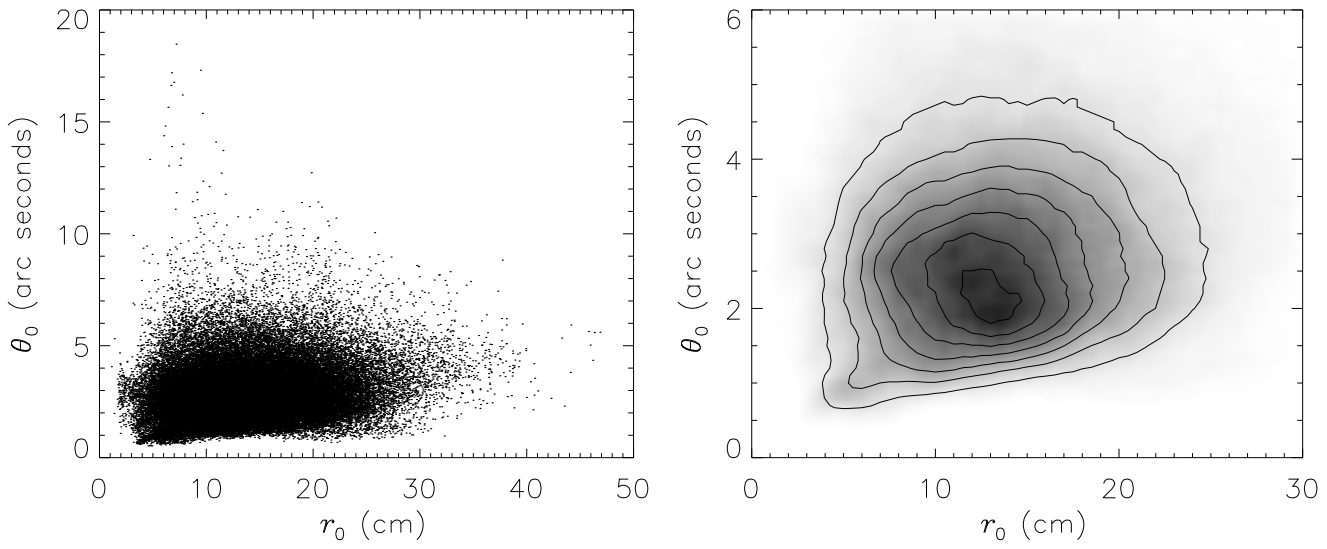

Figure 3: Scatter plot of the mutual r_0 and θ_0 distribution (left) and the central region of the joint histogram (right).

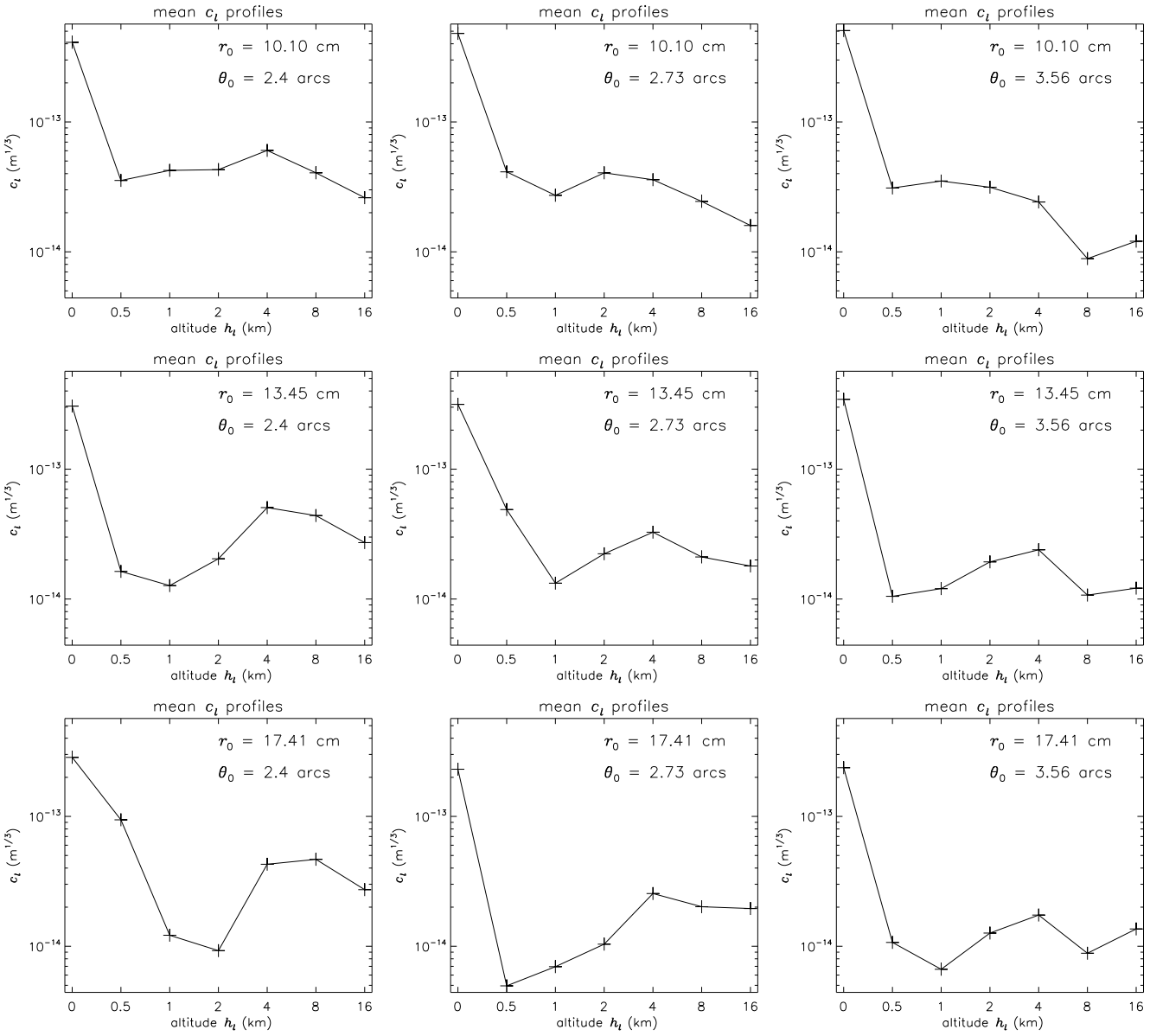

Figure 4: Mean c_l profiles computed for 3×3 rectangular bins defined in the two-dimensional r_0-θ_0 histogram (see Fig. 3).

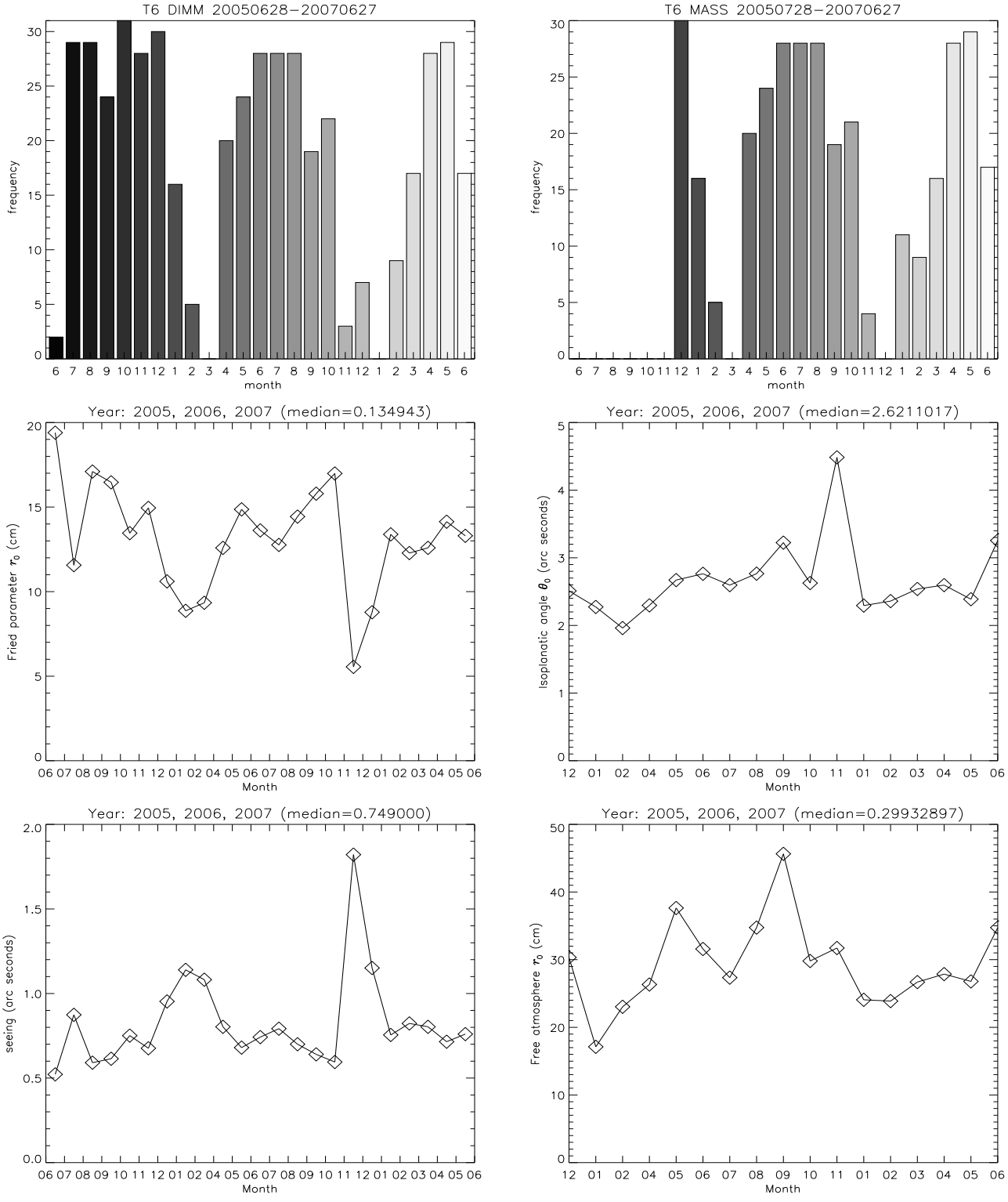

Figure 5: Monthly variations of the median Fried parameter and seeing (DIMM – left column), and the median isoplanatic angle θ_0 and free atmosphere $r0$ (MASS – right column), with the overall medians quoted in the title of each figure. The top row shows the monthly duty cycle (days per month) for each instrument.

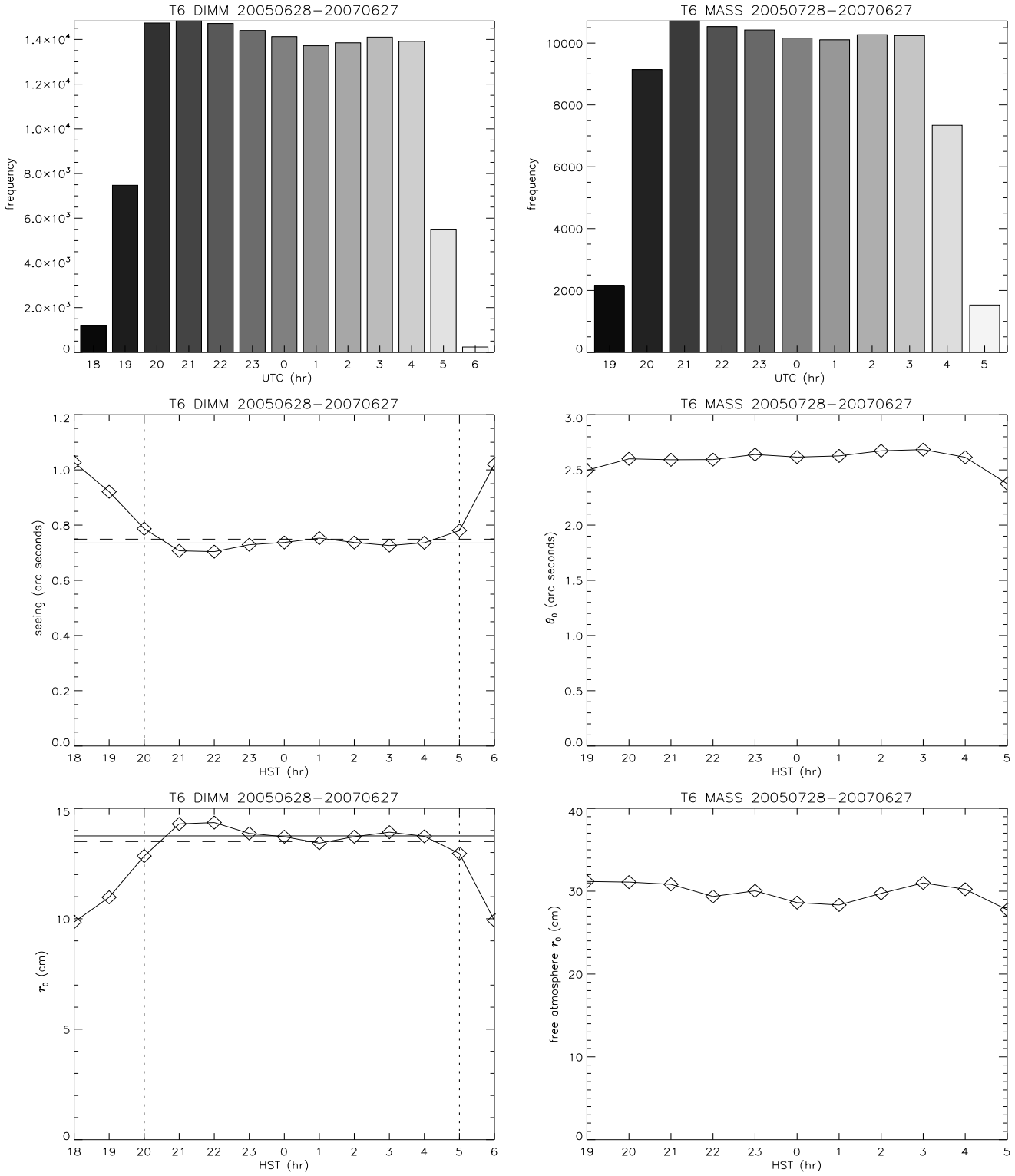

Figure 6: Hourly statistics of DIMM (left column) and MASS (right column) operations, referenced to the HST time zone (UTC-10). Top row shows the cumulative frequency of operation. For the seeing (right-middle) and r_0 (right-bottom) plots, the two horizontal lines indicate the total median value computed with (dashed) and without (solid) potential twilight hours included, as indicated by the two dotted vertical lines. For the MASS parameters this comparison produced almost no discernible difference, and was omitted from the plot.

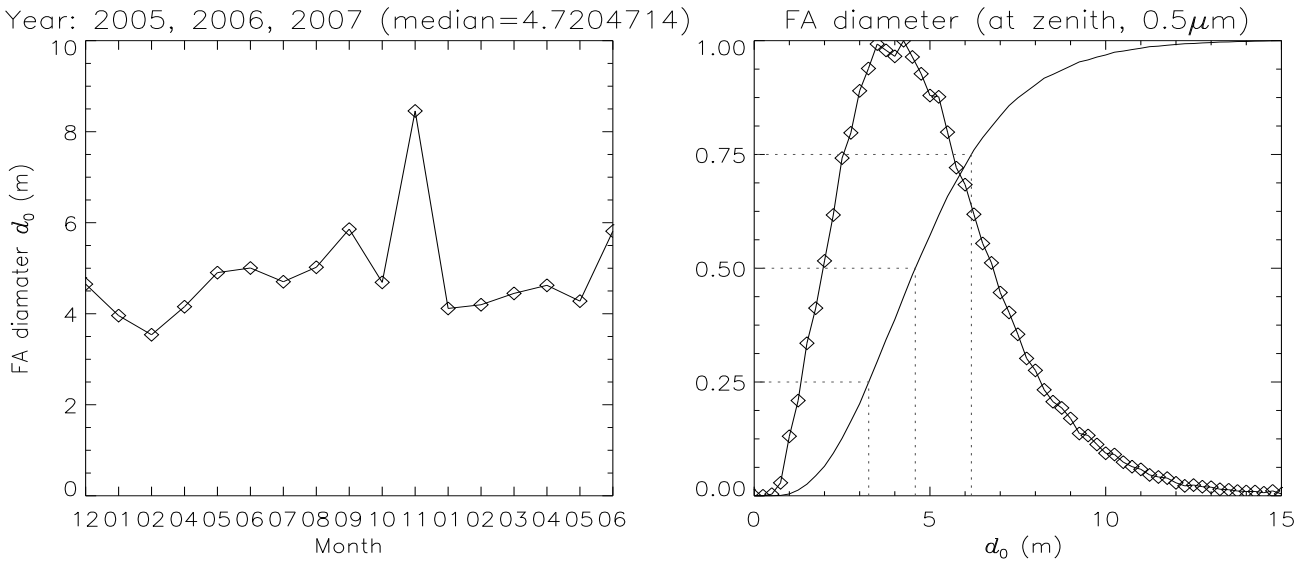

Figure 7: The focal anisoplanatism (FA) parameter d_0: monthly medians (left), and the overall histogram and cumulative density function (right). The 25th, 50th and 75th percentiles are indicated on the abscissa in the right figure by the dotted lines.

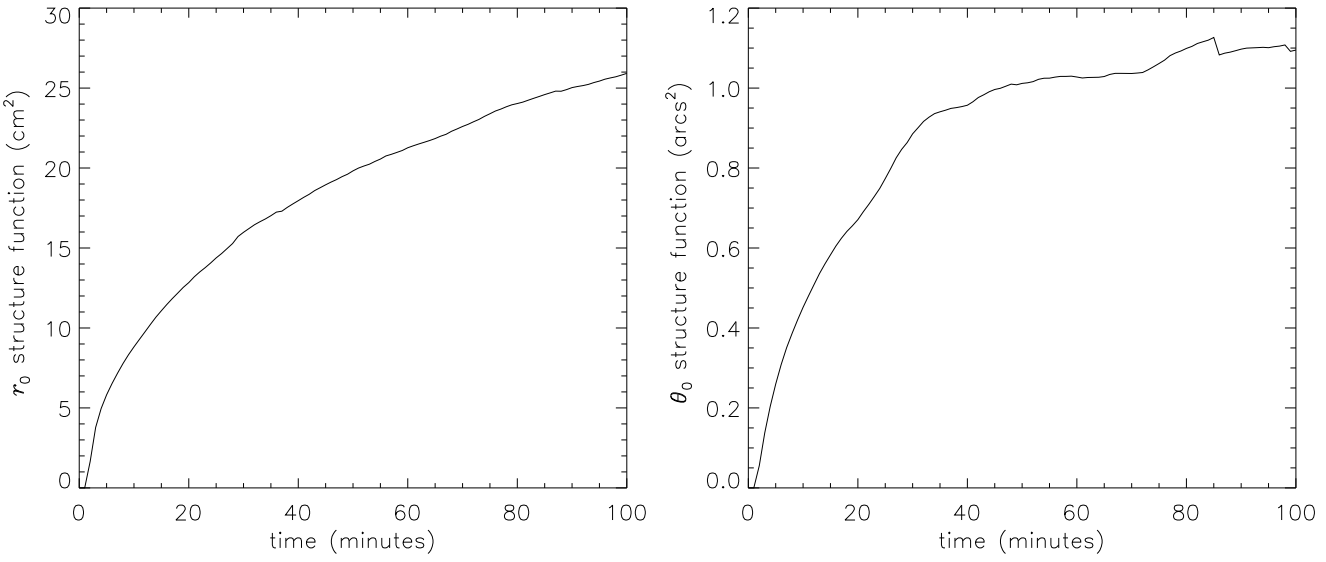

Figure 8: Structure functions of r_0 and θ_0. The θ_0 curve on the right is probably exhibiting some low number statistics as all data before December 2005 were discarded.

2 Addendum

This section was originally an unpublished addendum to KAON 415, which had looked at the 13N data by itself but did not compare with any seeing data taken from up on the summit ridge. For background on the 13N data set, see e.g. Refs. [1, 3]. Before the current study was undertaken, the underlying assumption was that the DIMM located at 13N might be adversely affected by additional ground-layer seeing, possibly resulting in a seeing environment significantly different from that experienced up on the summit. The driver for this study was the idea that, by correlating contemporaneous seeing measurements from the 13N DIMM and the summit observatories, this difference could be characterized and possibly turned into a useful summit seeing prediction/diagnostics tool based on 13N data. The results obtained here somewhat speak against that theory. The Subaru, UH and 13N seeing measurements were obtained with DIMM units (the Subaru DIMM is described in Ref. [5]; cf. e.g. Ref. [4] for information on the TMT site monitoring campaign and the 13N DIMM). The CFHT seeing data comprise measurements made with various instruments at the telescope (MegaPrime, WIRCam, AOB).

2.1 Normalizing the CFHT data

While the 13N, UH and Subaru data sets all came from DIMM units with the seeing values all referred to a common norm, e.g. zero zenith angle $\zeta = 0$ and a wavelength of $\lambda = 0.5$ μm, the CFHT data set had not been normalized to these conditions. Wavelength and air mass normalization were applied by the scaling factors $(\lambda_{\rm im}/\lambda)^{0.2}$ and $\cos^{0.6}(\zeta)$ respectively. The filter definitions for MegaPrime and WIRCam were obtained from: `http://www.cfht.hawaii.edu/Instruments/Filters/`.[1]

Less straightforward to define is the correction factor needed to account for measuring the seeing while guiding on a tip/tilt star, as was frequently the case with WIRCam and MegaPrime measurements. We applied a simple model that assumed that the ratio between guided and unguided FWHM could be modeled as the ratio between FWHM of analytically computed long-exposure (LE) and short-exposure (SE) PSFs. We use the analytical models (see e.g. Ref. [2]) for the MTF:

$$\langle S(f)_{\rm LE}\rangle = T(f)\,\exp\left[-\frac{1}{2}D(\lambda f)\right], \tag{1}$$

$$\langle S(f)_{\rm SE}\rangle = T(f)\,\exp\left\{-\frac{1}{2}D(\lambda f)\left[1-\left(\frac{\lambda f}{D}\right)^{1/3}\right]\right\}, \tag{2}$$

where $T(f)$ is the MTF of the diffraction-limited telescope and

$$D(r) = 6.88\left(\frac{r}{r_0}\right)^{5/3} \tag{3}$$

is the long-exposure Kolmogorov spatial structure function. We computed (1) and (2) for given telescope diameter and a range of r_0, obtained the PSFs by Fourier transform and measured the FWHM as a function of r_0. The two curves are shown in the left of Fig. 9. Plotting the short-exposure FWHM versus the long-exposure FWHM gives a linear relationship, as shown on the right in Fig. 9.. Fitting a linear function $g(\theta)$ to this relationship gives

$$g(\theta) = 0.0984689 + 1.14006\theta, \tag{4}$$

which was the correction term applied to the guided seeing measurements θ in order to estimate the unguided seeing value used for the statistical analysis.

2.2 Results

As a step towards understanding the seeing conditions on the Mauna Kea summit ridge, we would like to quantify systematic differences in seeing measurements obtained by different methods and at different sites. It is therefore necessary to use contemporaneous measurements for the study, which basically means performing the boolean `AND`

[1] For internal reference, the statistical analysis and all the described calibrations are implemented in the IDL code `mksee.pro` under the folder `/IDL.projects/MK-seeing/` on pakalana.

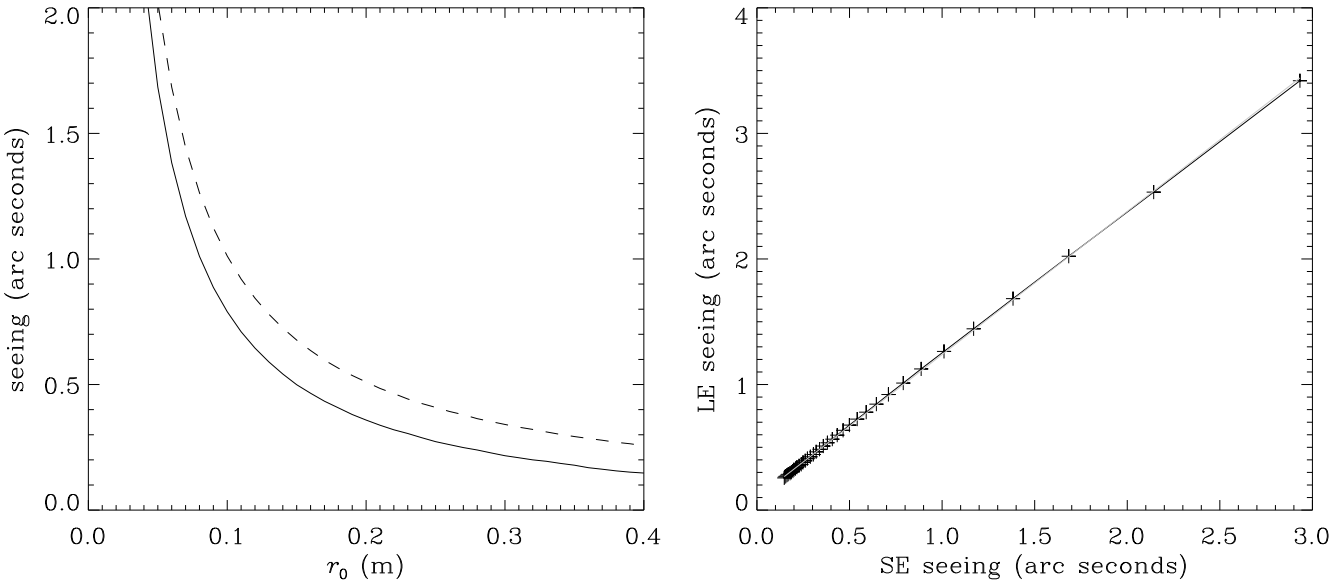

Figure 9: Left: FWHM from long-exposure (dashed line) and short-exposure (solid line) PSFs as a function of r_0. Right: linear relation between guided and unguided FWHM.

operation on the time stamps of the data sets, in order to extract the subsets of the data that were recorded (approximately) simultaneously. We proceed first by pairing up the 13N data to the other sets individually, the results of which are listed in table 1 and displayed in Fig. 10. Evidently we don't have a tight correlation between any of the data sets.

Continuing to extract the temporal union of all four data sets, we are left with comparatively few overlapping points. We can still compute the medians and histograms as shown in table 1 and Figs. 11 and 12, and bear in mind that the distributions can be expected to be a bit more noisy because of low number statistics. Also shown in Figs. 11 and 12 are curves fitted to the histograms assuming a log-normal function. The fit is typically poorer in the tail of the distribution, which is more pronounced than a log-normal distribution allows for.

2.3 Conclusions

We did not find a common systematic correlation between seeing measurements at four different locations on or near the Mauna Kea summit. This informs us that local conditions at each site (wind exposure, dome seeing, altitude) induce statistical differences that are as large as the difference between the summit ridge and the lower-altitude 13 North site. We have been investigating the possibility to add Keck seeing data to this study, but have not been able to collect the necessary data set. This sort of study should be repeated in the near future, as more seeing monitors go online and the data archives become populated.

correlation	data points	nights	range of dates	θ_{13N}	θ_{sub}	θ_{cfh}	θ_{uh}
13N–Subaru	35255	232	2005.07.08–2006.09.23	0.727	0.87	-	-
13N–CFHT	17737	215	2005.06.29–2006.09.23	0.73	-	0.89	-
13N–UH	16966	76	2005.07.16–2006.07.22	0.729	-	-	0.65
all	1759	38	2005.08.30–2006.07.07	0.70	0.91	0.89	0.69

Table 3: Summary of median seeing values measured in the correlation studies, and the quantity of data available in each correlation study. Seeing values are reported in arc seconds at zero zenith angle and at a wavelength of 0.5 μm.

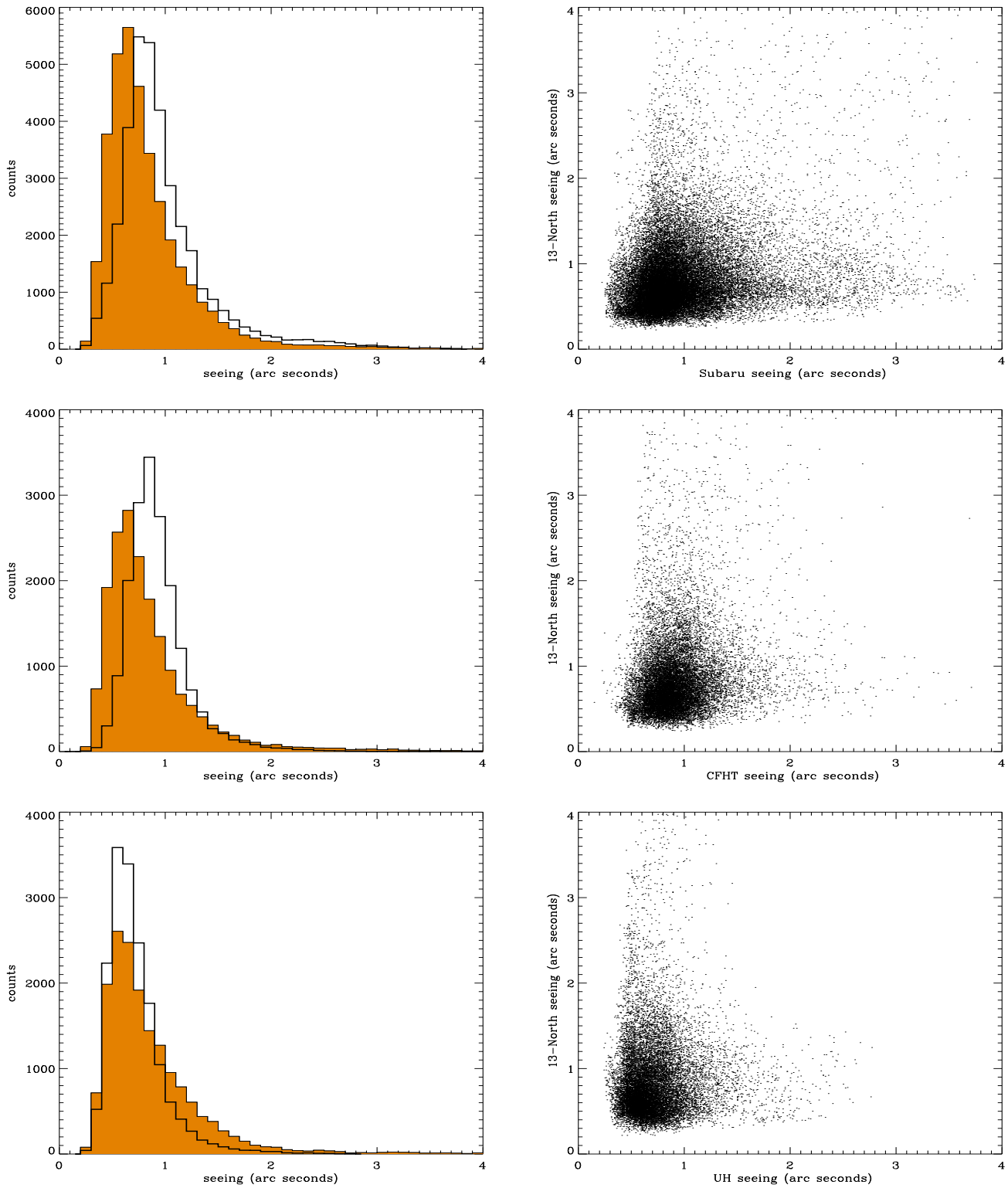

Figure 10: Seeing histograms (left) and correlation graphs (right) from correlating the 13N DIMM data to the Subaru (top), CFHT (middle) and UH (bottom) data sets, respectively. The filled histogram is 13N and the overplotted thick line the is respective correlated data set.

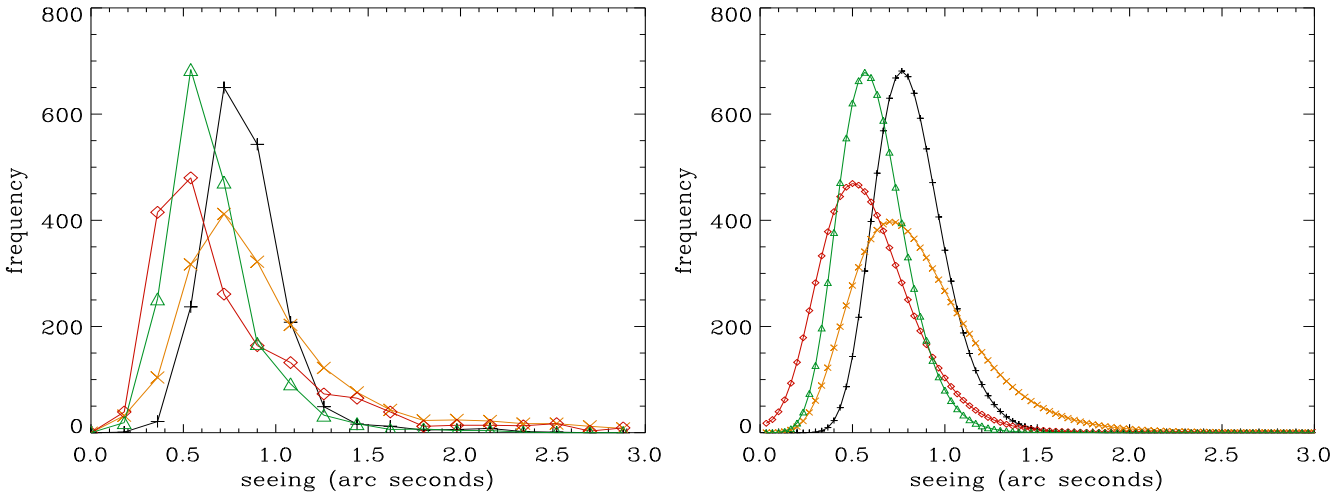

Figure 11: Seeing histograms (left) and log-normal curve-fits in the 4-way correlation study, with only 1759 overlapping data points. The curves are: CFHT (black plusses), Subaru (orange x's), 13N (red diamonds) and UH (green triangles). Also plotted individually in Fig. 12 for clarity.

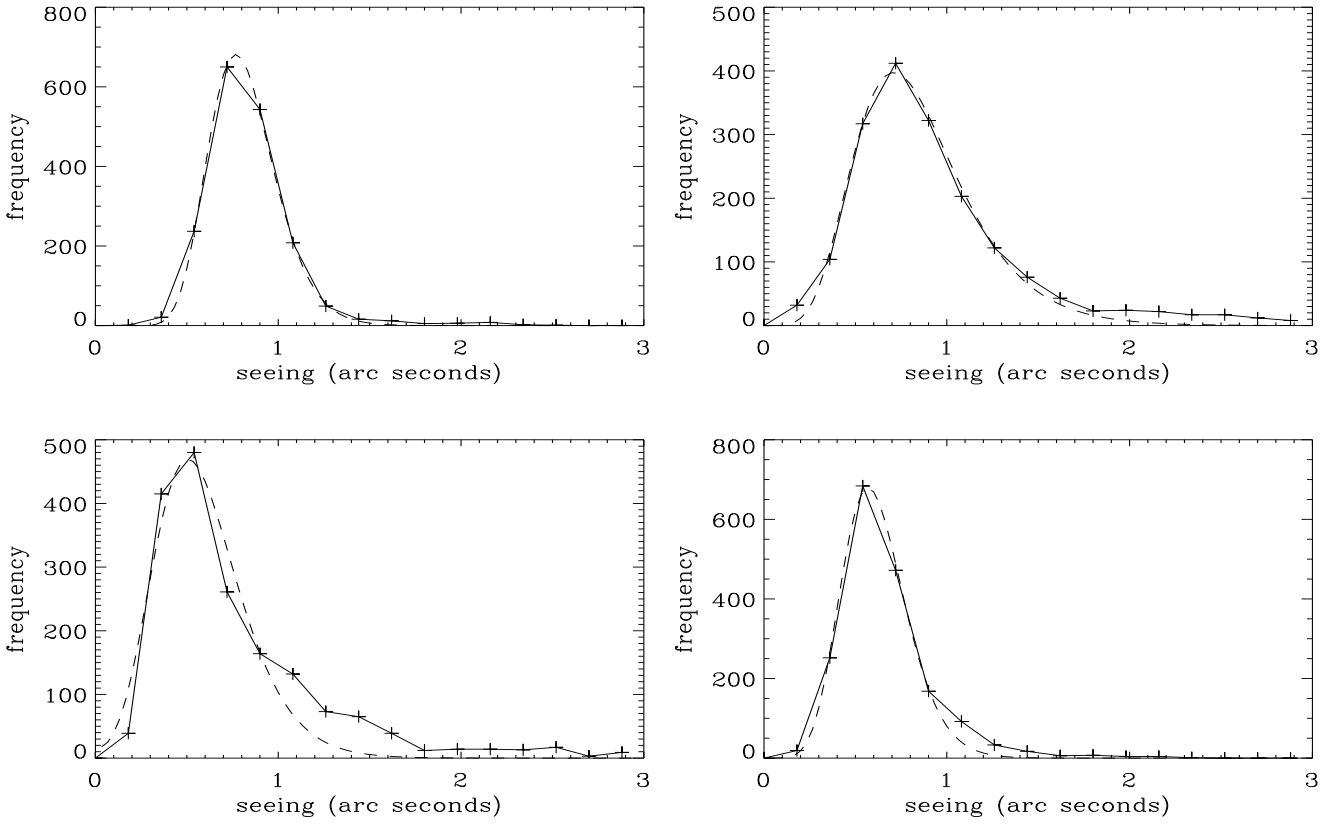

Figure 12: Seeing histograms and log-normal curve-fits in the 4-way correlation study, from left to right: CFHT, Subaru, 13N and UH.

Appendix

A Turbulence statistics formulae

The statistical quantities referred to in the text and in the graphs are defined here in their most common formulation. I have largely followed the definitions and notation of Ref. [2] (Hardy, 1998).

A.1 Turbulence moments

The m^{th} turbulence moment μ_m, and its upper and lower partial moments μ_m^+ and μ_m^-, are defined at zenith as

$$\mu_m = \int_0^\infty dh\, h^m\, C_n^2(h) \tag{5}$$

$$\mu_m^+(H) = \int_H^\infty dh\, h^m\, C_n^2(h) \tag{6}$$

$$\mu_m^-(H) = \int_0^H dh\, h^m\, C_n^2(h), \tag{7}$$

where h is the altitude variable, H is a given fixed altitude, and $C_n^2(h)$ is the refractive index structure constant (as a function of altitude) in units of $m^{-2/3}$. At non-zero zenith angles ζ the turbulence moments must be multiplied by $\sec^{m+1}(\zeta)$, but in order to make the zenith dependence explicit in the formulas of the next section, the term has been pulled out of the definition here. The m^{th} wind moment w_m is similarly defined as

$$w_m = \int_0^\infty dh\, v^{5/3}(h)\, C_n^2(h) \tag{8}$$

where $v(h)$ is the scalar wind speed as a function of altitude.

A.2 Statistical characterization

The temporal structure function D_φ of a stochastic variable φ is defined as

$$D_\varphi(\tau) = \langle \|\varphi(t+\tau) - \varphi(t)\|^2 \rangle. \tag{9}$$

Using the statistical moments given in Sect. A.1, the quantities most commonly used for describing turbulence statistics under Kolmogorov theory can be compactly formulated as:

$$r_0^{-5/3} = 0.423 k^2 \sec(\zeta)\, \mu_0 \tag{10}$$

$$\theta_0^{-5/3} = 2.914 k^2 (\sec\zeta)^{8/3}\, \mu_{5/3} \tag{11}$$

$$f_G^{5/3} = 0.102 k^2 \sec(\zeta) \int_0^\infty dh\, v^{5/3}(h)\, C_n^2(h) \tag{12}$$

$$d_0^{-5/3}(H) = k^2 \left[0.5\, \mu_{5/3}^-(H)\, H^{-5/3} - 0.452\, \mu_2^-(H)\, H^{-2} \right] \tag{13}$$

$$\tau_0 = 0.134 / f_G, \tag{14}$$

These quantities are known as the Fried parameter (r_0), the isoplanatic angle (θ_0), the Greenwood frequency (f_G), the focal anisoplanatism aperture d_0 and the coherence time (τ_0). The wavelength dependence enters through the wave number $k = 2!pi/\lambda$, and the LGS focal anisoplanatism (FA) parameter d_0 in Eqn. (13) has been simplified from its original expression under the assumption that μ_0^+ is negligibly small for sodium beacons at $H \leq 90$ km. Other useful expressions include the seeing-r_0 relationship

$$\theta = 0.98\, \frac{\lambda}{r_0}, \tag{15}$$

and inverting Eqn. (10) yields the 0^{th} order turbulence moment in terms of the Fried parameter:

$$\mu_0 = 0.06 \lambda^2 r_0^{-5/3}. \tag{16}$$

It is common in modeling and analysis of atmospheric turbulence for adaptive optics to use a discrete model of the atmosphere with a given number N_L of thin layers, by expressing the refractive index structure constant as

$$C_n^2(h) = \sum_{l=1}^{N_l} c_l \delta(h - h_l), \tag{17}$$

where δ is Dirac's delta function. The c_l coefficients represent the contribution to the integrated seeing from individual layers (in a convenient algebraic representation rather than physical) as obtained by integrating C_n^2 over a finite range:

$$c_l = \int_0^\infty dh\, g_l(h)\, C_n^2(h), \tag{18}$$

where $g_l(h)$ is an appropriate weighting function that asymptotes to zero (e.g. a linear spline, Gaussian, Hanning window, etc) and is centered on the altitude h_l. This is the intrinsic format on which the MASS unit does its estimation of $C_n^2(h)$, whereby it returns the coefficients c_l of a 6-layer profile starting from $h = 500$ meters. The MASS does not measure the ground layer, c_0, which must be obtained from a combination of DIMM and MASS data. In this study we computed the ground layer simply as

$$c_0 = \mu_0 - \sum_{l=1}^{N_L} c_l, \tag{19}$$

where μ_0 was computed from the DIMM seeing according to Eqns. (15) and (16). The isoplanatic angle is also easily computed from the MASS data by substituting (17) into (11), which gives

$$\theta = \left[2.941 k^2 \sum_{l=1}^{N_L} c_l h_l^{5/3} \right]^{-3/5}, \tag{20}$$

and an estimate of the free atmosphere seeing θ^* can be computed similarly as

$$\theta^* \approx \lambda \left[0.423 k^2 \sum_{l=1}^{N_L} c_l \right]^{3/5}, \tag{21}$$

References

[1] R. Flicker. Mauna Kea turbulence statistics from the TMT MASS/DIMM and weather station at the 13-North site. Technical Report KAON 415, W.M. Keck Observatory, 22 September 2006.

[2] J. W. Hardy. *Adaptive optics for Astronomical Telescope*. Oxford University Press, 1998.

[3] C. Neyman. *Accessing the Mauna Kea TMT seeing & weather data*. Keck note 2006-08-02, KPAOtech/SiteConditions/MaunaKeaSeeing/TMTmassdimmNotes.doc.

[4] W. Skidmore, M. Schöck, A. A. Tokovinin, G. Djorgovski, A. R. Walker, R. D. Blum, T. Travouillon, J. Seguel, E. E. Bustos, D. Walker, J. Vasquez, and P. E. Gillett. The Thirty Meter Telescope site testing system. In J. M. Oschmann, Jr., editor, *Proceedings of the SPIE, Volume 5489, pp. 154-164 (2004).*, pages 154–164, October 2004.

[5] F. Uraguchi, N. Takato, A. Miyashita, and T. Usuda. The DIMM station at Subaru Telescope. In *Ground-based and Airborne Telescopes. Edited by Stepp, Larry M.. Proceedings of the SPIE, Volume 6267, pp. (2006).*, July 2006.